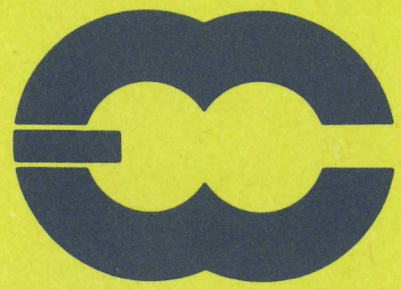

European Centre
for Medium Range
Weather Forecasts

Spurious Energy Conversions in an Energy/Enstrophy Conserving Finite Difference Scheme

Internal Report 22
Research Dept.

January 1979

Centre Européen pour les Prévisions Météorologiques
à Moyen Terme

Europäisches Zentrum für mittelfristige Wettervorhersage

Spurious energy conversions in an energy/enstrophy conserving finite difference scheme

By

A. Hollingsworth, P. Kållberg

European Centre for Medium Range Weather Forecasts
Shinfield Park, Reading, Berks.

Internal Report No.22

Research Department February 1979

N O T E :

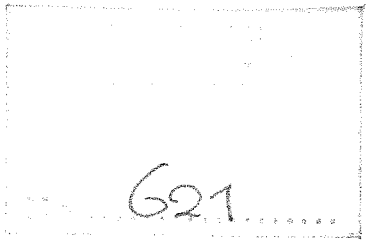

A B S T R A C T

Numerical experiments on real data were made with a finite difference scheme in advective form which conserved energy and which also conserved enstrophy for horizontal non divergent flow. Within a few days in a high resolution integration the strength of the jets decreased catastrophically with a large increase in short wave kinetic energy.

An analysis is made of the finite difference scheme, which shows that, when linearised about a non zero uniform flow, the finite difference equations do not conserve momentum and so do not have an energy theorem. Unstable free modes exist for each internal vertical mode while the external mode is stable. Thus a one-level analysis of the finite difference scheme would not reveal the problem. The growth rates 1) are zero if the flow is non-rotating, 2) are linearly proportional to the magnitude of the basic flow, 3) bear a roughly inverse relationship to the gravity speed of the vertical modes and 4) increase with decreasing grid size.

For a nine level model with a resolution of 200 km the e-folding time for the fastest growing disturbance is of the order of 6 hours when the mean flow velocity is 40 m/s.

Integrations with a non linear model in a simple situation show that the overall energy constraint is satisfied by a re-distribution of mass.

1. Introduction

The European Centre for Medium Range Weather Forecasts is developing a model suitable for medium range weather forecasts out to ten days. Two horizontal finite difference formulations of the model, originally due to Sadourny, have been described by Burridge and Haseler (1977) for the Arakawa "C" grid. One formulation has the property that it conserves the quantity Z/p*, where Z is the vertical component of absolute vorticity, for horizontal non-divergent flow in a one-level model. This scheme has been published in Sadourny (1975). The second scheme described by Burridge and Haseler is also due to Sadourny and conserves Z/p* under the same conditions; it further conserves energy in a general flow. We shall refer to these schemes as the E scheme (for the first) and the EE scheme (for the second).

The EE scheme was used in a real data integration in a high resolution ($\Delta\lambda = \Delta\theta = (\pi/2)/48$) model using both nine and fifteen levels in the vertical. After about two and a half days there was a dramatic collapse of the jets in the model with an accompanying rapid increase in short wave energy in the absence of dissipation. As a result, the integration lost all predictive value. This collapse did not occur when the E scheme was used. We present an analysis of the collapse which shows that non-conservation of momentum in the linearised equations in the EE scheme provides a spurious energy source in the linearised equations. Short wave-lengths can use this spurious energy source to grow exponentially with typical e-folding times of six hours. In simplified experiments to be described below, the overall energy constraint is satisfied by a redistribution of mass.

In Section 2 we describe the symptoms of the problem.

In Section 3 we present a qualitative analysis of the problem, in a one dimensional situation. This analysis is oversimplified but within its limitations it capture the main features of

the results from the more complete analysis presented in Section 4.

In Section 5 we describe some simple integrations and compare them with the analytical results from Section 4. In Section 6 we summarise and make some suggestions for further work.

2. Symptoms of the problem

Fig. 1 shows the 500 mb height field at days 2 and 3 in a nine-level integration from real data using the EE scheme and with no physical parameterisations. The field is truncated at zonal wave number twenty. Between the two days there has been a dramatic loss of intensity in the jets over the Pacific and Western Europe. If the integration is continued the fields degenerate into small scale noise by day seven. Integrations with either the dry convective adjustment used by Smagorinsky et al (1965) or with a complete set of physical parameterisations for radiation, the planetary boundary layer, dry convection, moist convection, large scale rain and internal diffusion showed the same collapse of the jets between day 2 and 3. Fig. 2 shows the evolution of the total kinetic energy in these three integrations. In the adiabatic integration the kinetic energy increases steadily with time. In the run with just the dry convection the kinetic energy stays more or less constant. In the third run the kinetic energy decreases steadily. This suggests that the model formulation is generating small scale noise which is exacerbated by convective overturning in the absence of the dry convection. When internal dissipation is included as well as the dry convection parameterisation this small scale noise is damped and we see the effect of the loss of energy in the longer waves.

Figs. 3 and 4 show the flow at days 3 and 4 in runs with the EE scheme (right half of frame) with the full suite of physical parameterisations and a similar run with the E scheme (left half of frame). There are no problems with the

E scheme; this integration continues to day 10 in a reasonable fashion. Both sets of fields have been truncated at zonal wave number twenty.

3. Qualitative analysis with a one level model

Consider the form of the shallow water equations on which both the E and EE schemes are based, viz.

$$\frac{\partial u}{\partial t} = Zv - \frac{\partial}{\partial x}(\phi + E) \tag{1}$$

$$\frac{\partial v}{\partial t} = -Zu - \frac{\partial}{\partial y}(\phi + E) \tag{2}$$

$$\frac{\partial \phi}{\partial t} = -\nabla . \phi \underline{U} \qquad \underline{U} = (\underline{i}u + \underline{j}v) \tag{3}$$

here $Z = f+\zeta$, f is the coriolis parameter, ζ the relative vorticity E is $(u^2+v^2)/2$ and the rest of the notation is standard.

These equations may be combined to form an energy theorem

$$\frac{\partial}{\partial t}\phi\left(\frac{u^2+v^2+\phi}{2}\right) + \nabla.\phi\left(\frac{u^2+v^2+\phi}{2}\right) = -\nabla.u\,(\phi^2/2) \tag{4}$$

Let us now linearise these equations about the following basic state

$$\bar{u} = \text{constant} \quad f = \text{constant}, \quad \bar{v} = 0, \quad \phi = \phi_o + \phi_1(y)$$

where

$$f\bar{u} = -\frac{\partial \phi_1}{\partial y}, \quad \bar{Z} = f, \text{and } \phi_o \text{ is constant.}$$

Then the linearised equations for x - independent perturbations are:

$$\frac{\partial u'}{\partial t} = \bar{Z}v' \tag{5}$$

$$\frac{\partial v'}{\partial t} = -\bar{Z}u' - Z'\bar{u} - \frac{\partial}{\partial y}\bar{u}u' - \frac{\partial \phi'}{\partial y} \tag{6}$$

$$\frac{\partial \phi'}{\partial t} = -\frac{\partial}{\partial y}\phi_o v' - \frac{\partial}{\partial y}\phi_1 v' \qquad (7)$$

In the v equation (equation 6) the terms $-Z'\bar{u} - \frac{\partial}{\partial y}\bar{u}u'$ cancel since $-z' = \frac{\partial u'}{\partial y}$.

If we assume that $\frac{\max(\phi_1)}{\phi_0} << 1$ then the term in ϕ_1 in the continuity equation may be neglected.

This assumption leads to the following simple system

$$\frac{\partial u'}{\partial t} = fv' \qquad (8)$$

$$\frac{\partial v'}{\partial t} = -fu' - \phi'_y \qquad (9)$$

$$\frac{\partial \phi'}{\partial t} = -\frac{\partial}{\partial y}\phi_o v' \qquad (10)$$

The energy theorem for this system is then

$$\frac{\partial}{\partial t}\left(\frac{u'^2+v'^2}{2} + \frac{\phi'^2}{2\phi_o}\right) = -\frac{\partial}{\partial y}\phi' v' \qquad (11)$$

Consider the EE finite difference form of the non-linear terms Zu and Zv in equations (1,2,3) as illustrated in Figs. 5a, 5b.

If we assume the same basic state as before and again neglect the term in ϕ_1, then the linearised form of the finite difference equations are

$$\frac{\partial u'}{\partial t} = f\overline{v'}^{y} \qquad (12)$$

$$\frac{\partial v'}{\partial t} = -f\overline{u'}^{y} - \frac{\bar{u}}{12}\left(2Z'_{j-1} + 8Z'_j + 2Z'_{j+1}\right) + \bar{u}Z'_j - \frac{\partial}{\partial y}\phi' \qquad (13)$$

$$\frac{\partial \phi'}{\partial t} = -\phi_o \frac{\partial}{\partial y} v' \qquad (14)$$

Here j-1, j, j+1 refer to the northern centre and southern latitude.

The terms corresponding to $-\frac{\bar{u}}{12}(2Z'_{j-1}+8Z'_j+2Z'_{j+1})+\bar{u}Z'_j$ in the v equation cancel in the continuous case. In the finite difference case they give

$$-\frac{\bar{u}}{12\Delta y}(-2u'_{j-2}-6u'_{j-1}+6u'_j+2u'_{j+1})-\frac{\bar{u}}{\Delta y}(u'_{j-1}-u'_j) \quad (16)$$

These do not cancel and in the special case of a three grid wave ($u'_{j-2}=u'_{j+1}$) the terms combine to give

$$-\frac{\bar{u}}{2\Delta y}(-u'_{j-1}+u'_j)=-\frac{\bar{u}}{2}Z'_j \quad (17)$$

For the rest of this qualitative analysis we concentrate on the special case of the three grid wave.

If we assume solutions proportional to $\exp(i\ell j\Delta y)$, $\ell=\pm\frac{2\pi}{3\Delta y}$ then equations 12, 13,14 become for a three grid wave

$$\frac{\partial u'}{\partial t}=\Gamma f v' \quad (18)$$

$$\frac{\partial v'}{\partial t}=\Gamma f u'-i\frac{\bar{u}}{2}\Lambda u'-i\Lambda\phi' \quad (19)$$

$$\frac{\partial \phi'}{\partial t}=-c^2 i\Lambda v \quad (20)$$

where $\Gamma=\cos(\ell\frac{\Delta y}{2})$, $\Lambda=\frac{\sin(\ell\frac{\Delta y}{2})}{(\frac{\Delta y}{2})}$ and we have $c^2=\phi_o$.

These equations may be combined into the following equation for v'

$$\frac{\partial^2 v'}{\partial t^2}=-(f^2\Gamma^2+c^2\Lambda^2)v'-i\frac{f\bar{u}\Gamma\Lambda}{2} \quad (21)$$

If we look for solutions proportional to $e^{\lambda t}$ then the dispersion relation is

$$\lambda^2=-(f^2\Gamma^2+\Lambda^2h^2)-i\frac{f\bar{u}\Gamma\Lambda}{2} \quad (22)$$

so that λ is complex. Without loss of generality we may take ℓ to be positive so that λ^2 lies in the lower left hand quadrant of the complex plane. Hence from Fig. 6 we see that one root has positive real part and so there is an exponentially growing solution. For c^2 sufficiently large, we see that the real part of this root is given by

$$\lambda_r = \frac{f\bar{u}\Gamma}{4c} \tag{23}$$

The e-folding times corresponding to the solutions of(22) with positive real part are shown in Fig. 7 for $\bar{u}$ = 40 ms^{-1} and f = 1.1 x 10^4 s^{-1}, for a range of values of c and Δy. We see that the growth rate increases with decreasing c and with decreasing Δy. At this point we reiterate that the analysis is merely suggestive because of the neglect of the term in ϕ_1. Large values of $\bar{u}$ correspond to large values of ϕ_1. The combination of small c and large $\bar{u}$ may therefore imply negative depth in the basic state. Such a state of affairs is physically unrealistic. In fact extensive testing of the EE scheme on the shallow water equations showed no indication of trouble (D.M. Burridge, personal communication). Nevertheless the tentative deductions that may be drawn from (23) are verified in the more complete analysis to be given below. These deductions are that a) the occurrence of instability requires that f be non zero, b) that the growth rate increases with increasing $\bar{u}$, c) that the fastest growth will occur for the smallest values of c in a multilevel model. Since in a multilevel model the smallest value of c corresponds to the mode with highest vertical wave number we expect the perturbations to have a two grid structure in the vertical.

At this point we may recall that in the E model the term Zu is written $-\bar{Z}^x\ \bar{u}^{xy}$. Hence the term $Z'\bar{u}$ has the finite difference expression $-(\bar{u}Z'_j)$, when $\frac{\partial}{\partial x} = 0$ and so it cancels exactly the term $-\delta_y \bar{u}u'$. Thus the linearised equations with this finite difference scheme have neither spurious momentum nor spurious energy sources.

4. Analysis for a multilevel model

We consider the primitive equations in sigma coordinates. We suppose that in the basic state the temperature is isothermal, with temperature T_o, and the uniform zonal flow $\bar{u}$ is balanced by a meridional pressure gradient $\bar{p}_*(y)$. We linearise about this basic state and consider perturbations for which $\frac{\partial}{\partial x} = 0$.

The finite difference equations and the notations may be found in Burridge and Haseler (1977). The derivation of the perturbation equations is straightforward.

As presented by Burridge and Haseler the finite difference scheme for the rotation terms applies to $[(\bar{p}_*^x u)(Z/\bar{p}_*^{xy})]$ and $[(\bar{p}_*^y v)(Z/\bar{p}_*^{xy})]$. It was found in the nonlinear model discussed later that the instability was not affected by these terms in p_* and so we present here the equations and results for the slightly simpler scheme for $[uZ]$ and $[vZ]$. The linearised equations are then

$$\frac{\partial}{\partial t} p'_{*j} = -\sum_{\ell=1}^{N} \left[v'_{\ell j} \frac{\bar{p}_{*j-1}+\bar{p}_{*j}}{2\Delta y} - v'_{\ell j+1} \frac{\bar{p}_{*j}+\bar{p}_{*j+1}}{2\Delta y} \right] \Delta\sigma_\ell \qquad (24)$$

$$\frac{\partial}{\partial t} T'_{kj} = \frac{\kappa \bar{T}}{\bar{p}_{*j}} \left(\frac{\Delta \ell n \sigma}{\Delta \sigma}\right)_k \left[\sum_{\ell=1}^{k-1} \left(-v'_{\ell j} \frac{\bar{p}_{*j-1}+\bar{p}_{*j}}{2\Delta y} + v'_{\ell j+1} \frac{\bar{p}_{*j}+\bar{p}_{*j+1}}{2\Delta y} \right) \Delta\sigma_\ell \right.$$

$$\left. + 0.5 \left(-v'_{kj} \frac{\bar{p}_{*j-1}+\bar{p}_{*j}}{2\Delta y} + v'_{kj+1} \frac{\bar{p}_{*j}+\bar{p}_{*j+1}}{2\Delta y} \right) \Delta\sigma_k \right] \qquad (25)$$

$$+0.5 \frac{\kappa \bar{T}}{\bar{p}_{*j}} \left[v'_{kj} \frac{\bar{p}_{*j-1}+\bar{p}_{*j}}{2} \frac{\overline{\ell n p_{*j-1}} - \overline{\ell n p_{*j}}}{\Delta y} + v'_{kj} \frac{\bar{p}_{*j}+\bar{p}_{*j+1}}{2} \frac{\overline{\ell n p_{*j}} - \overline{\ell n p_{*j+1}}}{\Delta y} \right]$$

$$\frac{\partial}{\partial t} u'_{kj} = \frac{f}{2}(v'_{kj}+v'_{kj+1}) \qquad (26)$$

$$\frac{\partial}{\partial t} v'_{kj} = -\frac{f}{2}(u'_{kj-1}+u'_{kj}) + \frac{\bar{u}}{12\Delta y}\left[2u'_{kj-2}+6u'_{kj-1}-6u'_{kj}-2u'_{kj+1}\right]$$

$$-\frac{\bar{u}}{\Delta y}\left[u'_{kj-1}-u'_{kj}\right]$$

$$-R\left[\sum_{\ell=k+1}^{K} T'_{\ell j-1}\frac{(\Delta \ln\sigma)}{\Delta y}_{\ell} + \frac{1}{2}T'_{kj-1}\frac{(\Delta \ln\sigma)}{\Delta y}_{k}\right]$$

$$+R\left[\sum_{\ell=k+1}^{K} T'_{\ell j}\frac{(\Delta \ln\sigma)}{\Delta y}_{\ell} + \frac{1}{2}T'_{kj}\frac{(\Delta \ln\sigma)}{\Delta y}_{k}\right]$$

$$-\frac{\bar{RT}}{\Delta y}\left[\frac{p'_{*j-1}}{\bar{p}_{*j-1}} - \frac{p'_{*j}}{\bar{p}_{*j}}\right]$$

$$-\frac{R}{2}(T'_{kj-1}+T'_{kj})\frac{\overline{\ln p_{*j-1}} - \overline{\ln p_{*j}}}{\Delta y} \qquad (27)$$

In equation (27) we have used the following linearisation for $\ln(p_*)$

$$\ln(\bar{p}_{*j} + p'_{*j}) = (\ln\bar{p}_*)_j + \ln(1+p'_{*j}/\bar{p}_{*j}) \approx \overline{\ln p_{*j}} + p'_{*j}/\bar{p}_{*j}$$

In equations (24) - (27), K is the total number of levels, j-1, j, j+1 indicate rows in the meridional direction. It remains only to specify boundary conditions. For the analytic calculation we require that the solution be periodic with period $N\Delta y$. This simplifies the calculation. Thus we have $(3k+1)N$ equations for $(3k+1)N$ unknowns.

The problem could be much simplified if it were separable. This is not the case because of the variation of the mean pressure field.

We therefore write the problem in the form

$$\frac{dX}{dt} = AX \qquad (28)$$

where X is a column vector of all the perturbation quantities and the matrix A contains the dependencies on the parameters of the problem. The eigenvalues of A give the frequencies of the free modes of the problem and the eigenfunctions give the structure of the free modes. The eigenvalues and eigenfunctions were calculated using routines from the NAG library.

Of the (3k+1)N solutions, N will have zero frequencies corresponding to steady state solutions. A further kN will also have zero frequency corresponding to the Rossby wave solutions. These are of course forbidden by either of our assumptions f = constant and $\frac{\partial}{\partial x} = 0$. The remaining 2kN solutions will correspond to gravity waves.

We would now like to identify the vertical mode to which each of these frequencies corresponds. For our 5 level model the gravity wave speeds for a resting basic state were 312.32, 143.4, 56.85, 26.07, 10.98 m/s. Using the ratios of these speeds to each other in an inspection of the eigenfrequencies of (28) it was possible to identify unambiguously the solutions corresponding to each mode in the vertical. Each vertical mode has N frequencies of positive sign and N frequencies of negative sign. The difference in sign of the frequency corresponds to a phase shift of half a wave length (or of northward and southward phase velocity). The N frequencies of one sign correspond to the N degrees of freedom in the separable problem.

The analysis of the previous section dealt only with the case N=3. However it is clear that the non-cancellation will occur for any value of $N \geq 3$. We have calculated the

eigenvalues and the fastest growing eigenfunction for the following range of situations:

a) 2 equally spaced levels $3 \leq N \leq 25$

b) 5 equally spaced levels $3 \leq N \leq 12$

c) 9 levels as used by Smagorinsky et al (1975) $3 \leq N \leq 8$.

The solutions for N = 3,4 were quite typical of the unstable modes.

As N increased eigenfrequencies corresponding to N = 3(or 4) were always found when N was a multiple of 3 (or 4). They were not always the fastest growing mode but the structure of the fastest growing mode was always quite similar. For example when N = 8 (or N = 6) the fastest growing mode had a structure very close to the solution for N = 4 (or N = 3) in one half of the domain and was precisely out of phase in the other half. The differences in growth rate of the fastest growing mode for N = 4 and N = 8 (or N = 3 and N = 6) was of the order of a few percent. For this reason we confine ourselves to the discussion of the structures of the unstable modes to the cases N = 3 or N = 4.

A striking feature of the results was that for each vertical mode there were exponentially growing free solutions, except for the external mode which was always neutral.

As expected, the most rapidly growing mode was the highest internal mode. As the vertical wave length decreased the growth rate decreased, as expected. Figs. 8, 9 show the dependence of the growth rate of the fastest growing modes corresponding to each internal mode for N = 3, N = 4 as $\bar{u}$ is varied from 0 to 40 m/sec, in a model with five equally spaced levels and Δy = 100 km. The growth rate is almost exactly linear in $\bar{u}$. At $\bar{u}$ = 40 m/sec the e-folding times in this model are of the order of 6 hours.

In Fig. 10 we show the variation of growth rate with Δy for the fastest growing mode in two models, one with 5 equally spaced levels and one with 9 levels as in the GFDL model referred to earlier. In both cases we find a marked variation of growth rate with horizontal grid size. The nine level model has larger growth rates and more sensitivity to Δy. The slowest moving gravity wave in the nine level model has a phase speed of 2 m/sec as compared to 10.58 m/sec in the five level model. In particular we note that the e-folding time decreases by a factor of two from 12 hours to 6 hours in the nine level model as Δy is changed from 400 km to 200 km. This is consistent with the rapid decay of the jets in the high resolution model compared to the much slower decay in a model with a resolution of 3.75^{o}, the highest resolution previously tested. In the latter case the decay of the jets over a period of several days had been ascribed the coarse horizontal resolution. In Figs. 11 and 12 we show the structures of the most unstable mode for N = 3, N = 4 in the 5-level model with $\bar{u}$ = 40 m/sec. In each case there are four zero crossings in the v-field so that we do indeed have the highest vertical mode.

The energy budget of the linearised perturbations is outlined in the next section.

Since the terms involving f in the equations for u' and v' would cancel exactly in the absence of the remaining terms it is clear that the energy source for the perturbations lies in the terms $- z' \bar{u} - \frac{\partial}{\partial y} \bar{u}u'$ which cancel in the continuous case.

5. Nonlinear integrations

In this section we present some results on integrations with a full model for the simple initial states discussed earlier. The model has been described by Källberg (1977). The flow is in a channel on an f-plane between rigid walls and

variations in the east-west direction are suppressed. The presence of the boundaries at the north and south might be thought to weaken the relevance of the analysis of Section 4, which assumed periodicity in the north south; this proves not to be the case.

The integrations were made with a model which had five equally spaced levels in the vertical and 32 points in the north south with a grid size of 100 km. The initial state consisted of an isothermal atmosphere with a uniform zonal flow of 40 m/s at all levels. The zonal flow was balanced by a meridional pressure gradient. To this was added a perturbation of 1 m/sec in the v-field. The integration proceeded without any significant features for two days. On day three we began to see a significant distortion of the zonal flow. The wind field on day 3 is shown in Fig. 13 for the levels 4 and 5 (700 mb and 900 mb). There are several bands of convergence and divergence at each level and a close inspection shows that the convergences and divergences have opposite signs between layers. The dominant wave number appears to be 4. This presumably is related to the number of points in the grid.

Fig. 14 shows the corresponding picture for day 4. We see that the zonal flow has been completely disrupted. The integration, which should have preserved a zonal flow of 40 m/sec with some small perturbations, has gone completely awry with easterlies and westerlies in excess of 60 m/sec.

A plot of the evolution of the rms divergence field in the period day three to four shows that the divergence is growing exponentially in time with an estimated e-folding time of 6.46 hours. The calculated e-folding time for a disturbance on this flow is 6.64 hours, if the north south periodicity is 4 grid points, and is 6.42 hours if the north south periodicity is 8 grid points. The agreement in the structure and growth rate of the disturbance with the

analytic calculation is sufficiently close to enable one to conclude that the analytic calculation has captured the main features of the disturbance in the model.

From the analytic results we could calculate the contributions of the terms in p'_s, u', T' to the v energy and the term in v' to the growth in the u' energy. In the equation for $(v')^2$ the surface pressure term contributed zero and the terms in u', T' were in the ratio .52 to .26 with the contribution from the T' term negative, implying that the combination of the perturbation geopotential term and the term in $RT' \frac{\partial}{\partial y} \overline{\ln ps}$ was tending to inhibit the growth. The term in u' in the $(v')^2$ equation as compared with the term in v' in the $(u')^2$ equation was .52 to .02. Clearly then the source of the energy for the perturbation is the non-cancellation of the terms $- Z' \bar{u} - \frac{\partial}{\partial y} \bar{u}u'$ as discussed earlier.

The non-linear integrations conserved total energy and the mean temperature was essentially constant during the course of the integration. However, the surface pressure field was changed radically. The initial north south pressure gradient gave surface pressure on the northern boundary of 920 mb and 1090 mb on the southern boundary. By day five the surface pressure field consisted of a uniform value of 1000 mb everywhere on which were superimposed variations of short wave length of the order of 25 mb. Thus energy conservation was ensured by a redistribution of mass.

6. Summary and conclusions

The energy enstrophy-conserving finite difference in advective form described earlier gave rise to a dramatic destruction of the jet streams when used in an integration on real data. The source of the problem has been identified as a non-conservation of momentum in the linearised equations. Integrations with a closely related enstrophy

conserving scheme give reasonable results in a real data forecast. The linearised equations for this latter scheme do conserve momentum. The problem of non-conservation of momentum in the linearised equations does not arise in an energy enstrophy conserving scheme written in flux form such as that described by Arakawa and Lamb (1977). However, a semi-implicit time scheme is much easier to implement with the equations in advective form rather than flux form. For the immediate future we shall use the enstrophy conserving scheme in our forecast experiments. Renner (personal communication) has proposed a re-definition of the term ∇E of the mass fluxes which eliminates the non-cancellation in the linearised equations. This proposal is being tested.

Some further aspects of the results are worth commenting on. Clearly a study of the linearised energetics of a finite difference scheme is of importance before using the scheme in a full model. In the present case the overall constraint of energy conservation was of little relevance for the growth of the instability. The dynamics of the disturbance is essentially linear.

Secondly we have here a demonstration of the limitations of one-level models for testing of finite difference schemes. In the present case the external mode is stable while the internal modes are all unstable, with largest growth rates for the highest internal modes. Since the external mode is stable, a one-level model will suggest that the scheme is stable when in fact is gives unstable results in a multi-level model.

Acknowledgements: Thanks are due to Clive Temperton who calculated the gravity wave speeds for the various models. The many lively discussions with David Burridge and Lennart Bengtsson were of great benefit. The typing and drafting were most competently executed by Mrs A. Dinshawe, Mrs I. Rhodes and Ms R. Shambrook.

References

Arakawa, A. and Lamb,V.R. 1977 "Computational design of the basic dynamical processes of the UCLA general circulation model" in "Methods in Computational Physics". Vol 17 Ed. J. Chang, Academic Press

Burridge, D.M. and Haseler, J.C. 1977 A model for medium range weather forecasting. Technical Report 4 ECMWF, Bracknell.

Källberg, P. 1977 A channel version of the ECMWF grid point model. Internal Report 16 ECMWF, Bracknell.

Sadourny, R. 1965 The dynamics of finite difference models of the shallow water equations. J.Atmos.Sci. 32 680-689.

Smagorinsky, J. et al 1965 Numerical results from a nine level general circulation model of the atmosphere. Mon.Wea.Rev. 93 727-768.

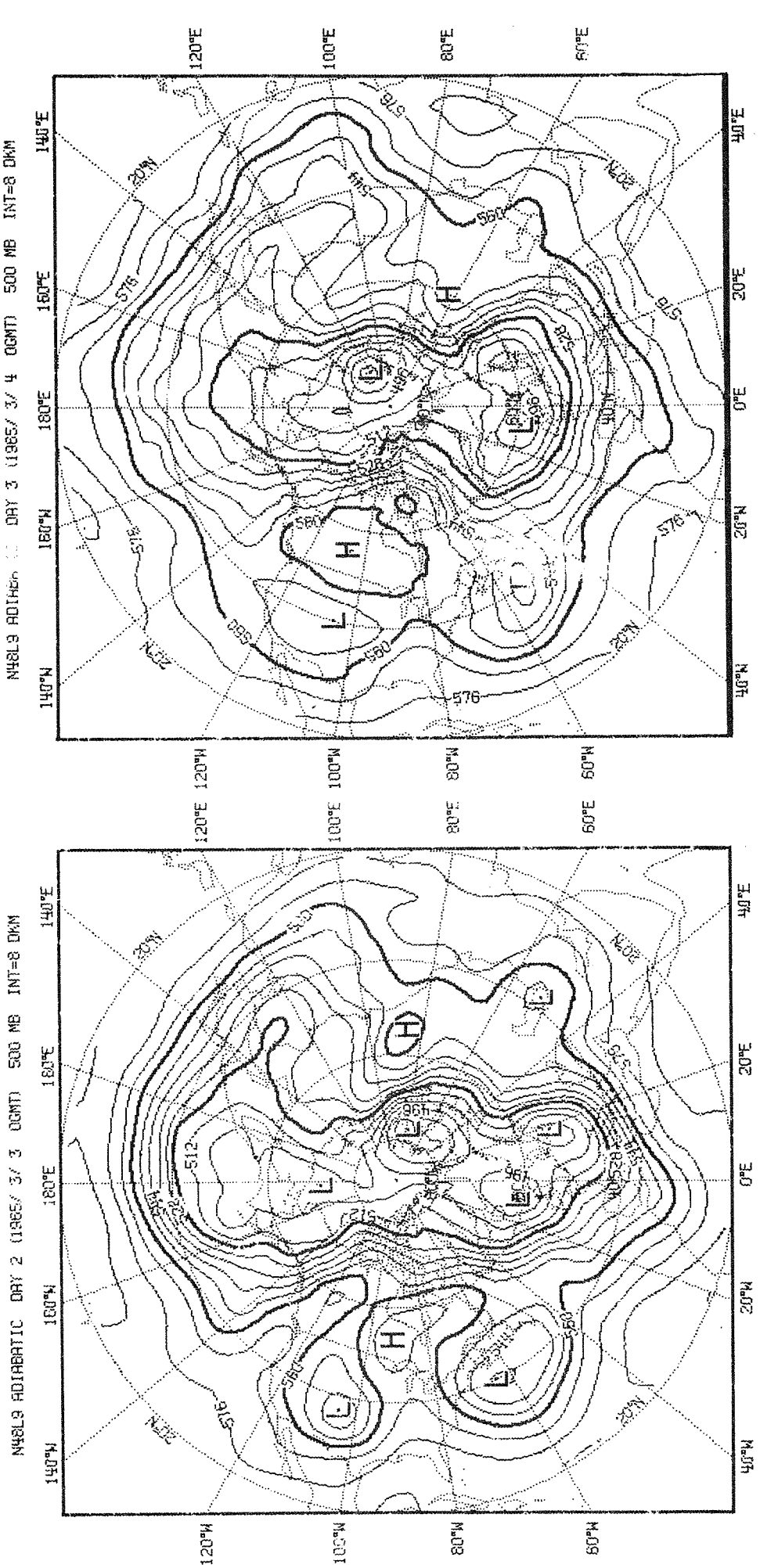

Fig. 1 500mb fields at day 2 (left) and 3 (right) in a run with the EE formulation and no physical parameterisations. The fields have been truncated at zonal wave number twenty.

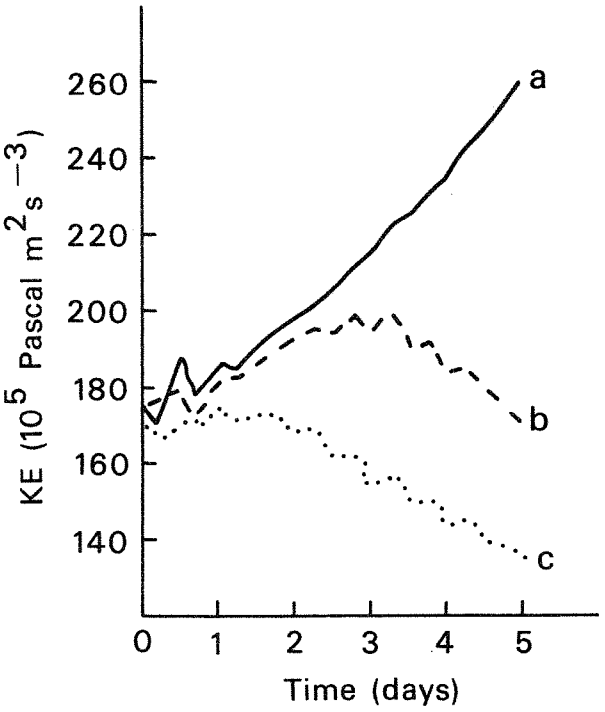

Fig. 2 Time evolution of the kinetic energy in three high resolution integrations from the same data using the EE formulation

a: adiabatic integration

b: integration with dry convection parameterisation

c: integration with full suite of physical parameterisations

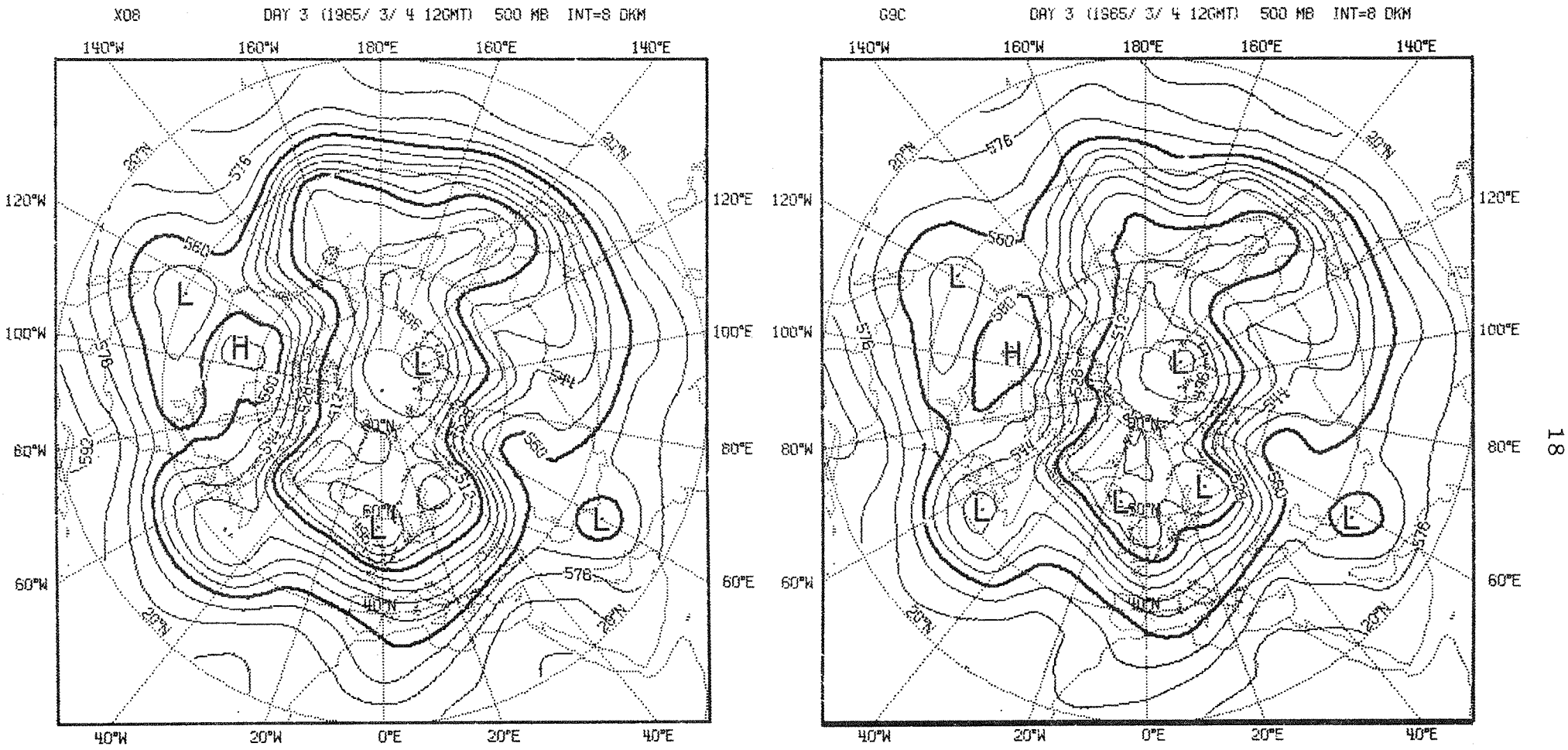

Fig. 3 500mb maps at day 3 in runs with EE scheme (right) and E scheme (left). Both runs had a full suite of physical parameterisations. The fields were truncated at wave number twenty.

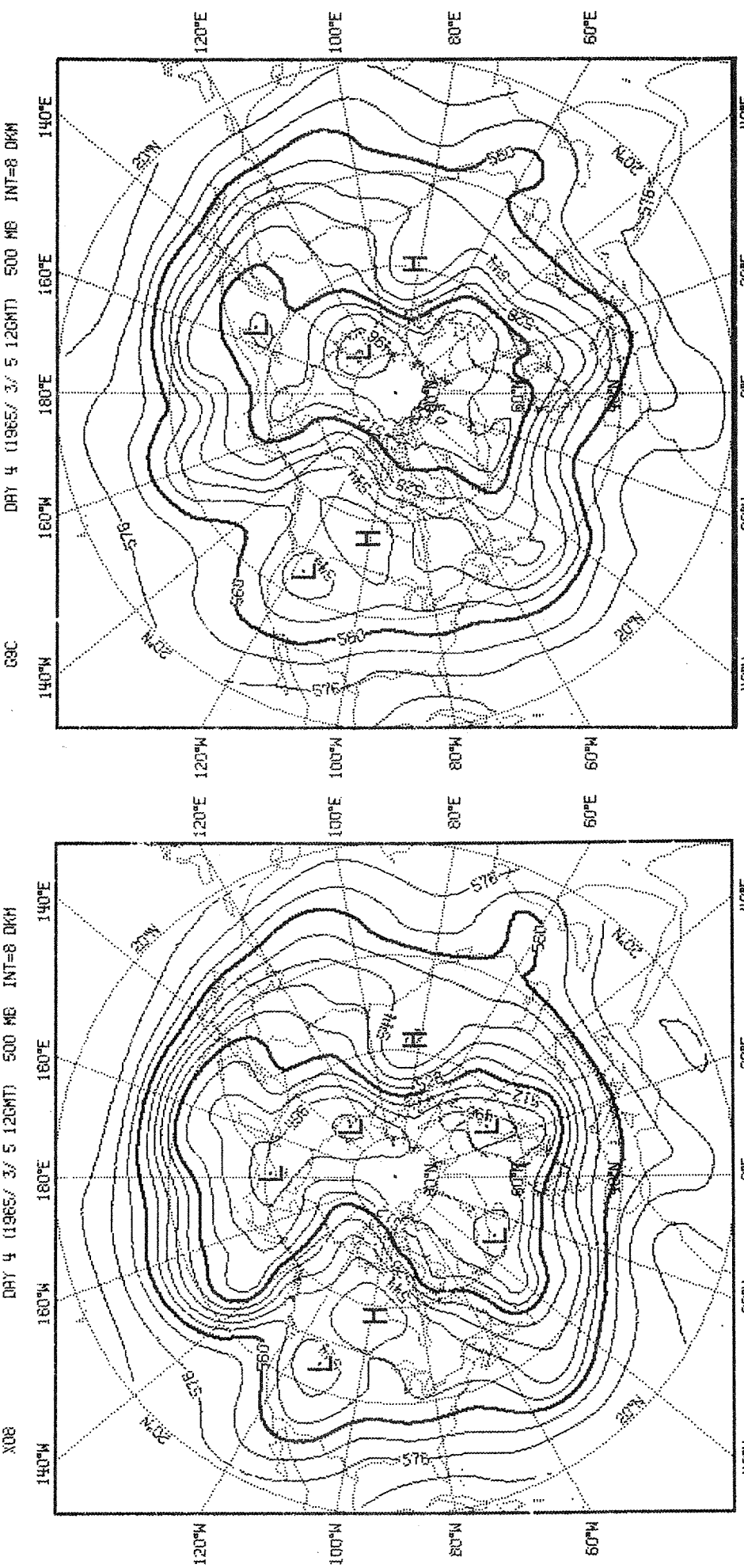

Fig. 4 As Fig. 3 at day 4 for the same integrations.

$$\left[\underline{\ } ZV\cos(\theta) \underline{\ }\right]_{oo} = \tfrac{1}{4}\left[\underline{\ }(V\cos(\theta))_{\frac{1}{2},\frac{1}{2}}(Z_{o,\frac{1}{2}}+Z_{o,-\frac{1}{2}}+Z_{1,\frac{1}{2}})/3\right.$$

$$+(V\cos(\theta))_{-\frac{1}{2},\frac{1}{2}}(Z_{o,\frac{1}{2}}+Z_{o,-\frac{1}{2}}+Z_{-1,\frac{1}{2}})/3$$

$$+(V\cos(\theta))_{-\frac{1}{2},-\frac{1}{2}}(Z_{o,\frac{1}{2}}+Z_{o,-\frac{1}{2}}+Z_{-1,-\frac{1}{2}})/3$$

$$\left.+(V\cos(\theta))_{\frac{1}{2},-\frac{1}{2}}(Z_{o,\frac{1}{2}}+Z_{o,-\frac{1}{2}}+Z_{1,-\frac{1}{2}})/3 \quad \underline{\ }\right]$$

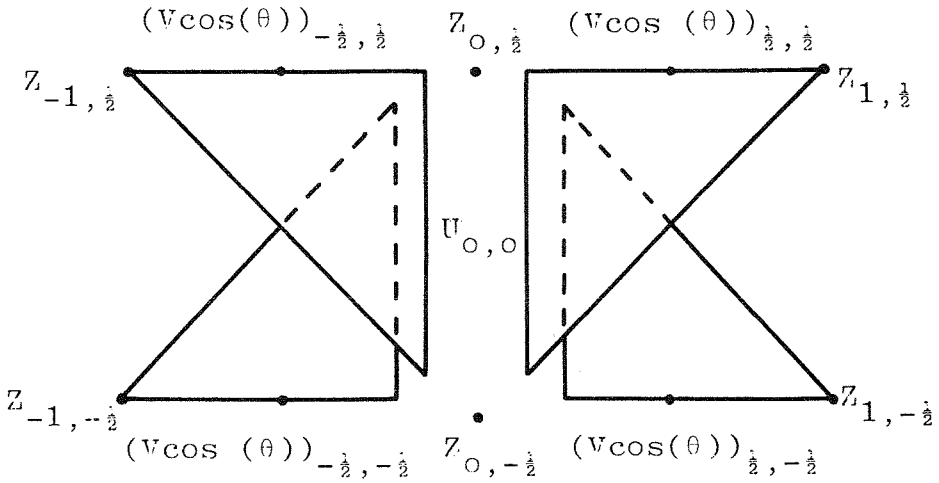

Fig. 5a Formulation of the term $\left[\underline{\ } ZV \underline{\ }\right]$.

$$\left[\overline{\underline{ZU}}\right]_{o,o} = \tfrac{1}{4}\Big[\overline{\underline{U}}_{\frac{1}{2},\frac{1}{2}}(Z_{-\frac{1}{2},o}+Z_{\frac{1}{2},o}+Z_{\frac{1}{2},1})/3$$

$$+U_{-\frac{1}{2},\frac{1}{2}}(Z_{-\frac{1}{2},o}+Z_{\frac{1}{2},o}+Z_{-\frac{1}{2},1})/3$$

$$+U_{-\frac{1}{2},-\frac{1}{2}}(Z_{-\frac{1}{2},o}+Z_{\frac{1}{2},o}+Z_{-\frac{1}{2},-1})/3$$

$$+U_{\frac{1}{2},-\frac{1}{2}}(Z_{-\frac{1}{2},o}+Z_{\frac{1}{2},o}+Z_{\frac{1}{2},-1})/3\Big]$$

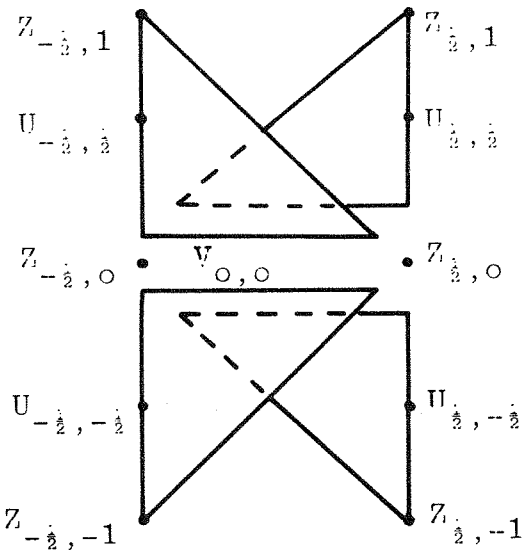

Fig. 5b Formulation of the term $\left[\overline{\underline{ZU}}\right]$.

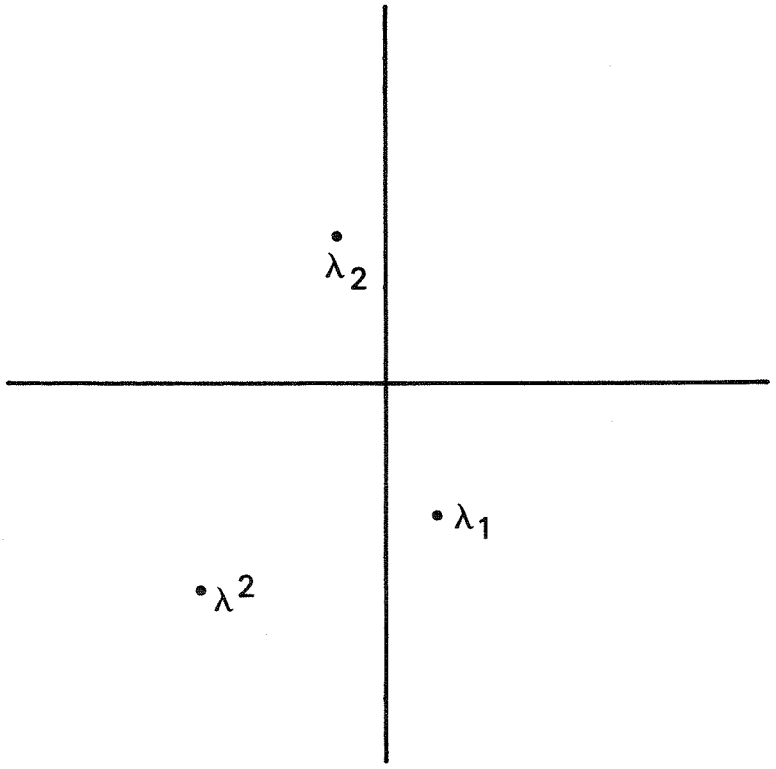

Fig. 6 Schematic of the position on the complex plane of λ^2 and its two roots λ_1 λ_2 where λ^2 is given by (22) with $\ell > 0$.

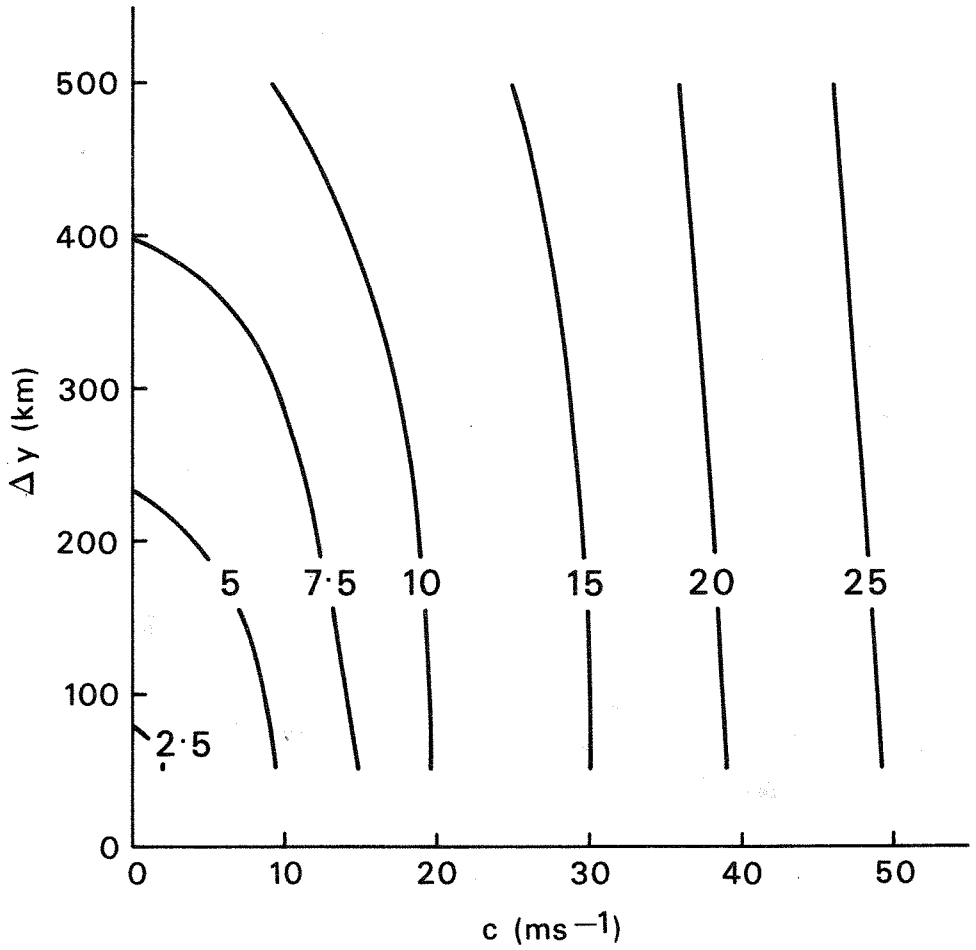

Fig. 7 e-folding time in hours for the unstable solutions of equation 22 for 1 $ms^{-1} \leqslant c \leqslant 50\ ms^{-1}$ and 50 km $\leqslant \Delta y \leqslant$ 500 km.

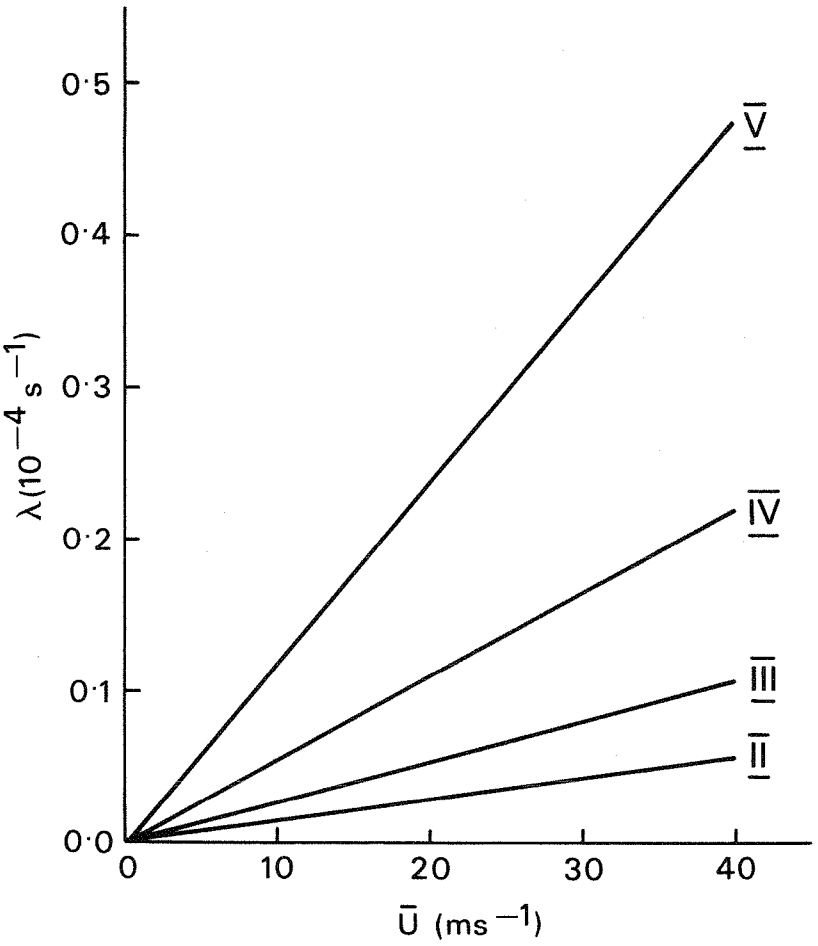

Fig. 8 Growth rate as a function of $\bar{U}$ for the four internal modes when N = 3 (i.e. the north south period is $3\Delta y$). The curves are labelled II, III, IV, V in order of decreasing gravity wave speed.
$f = 1.1 \times 10^{-4}$, Δy = 100 km, 5 equally spaced levels.

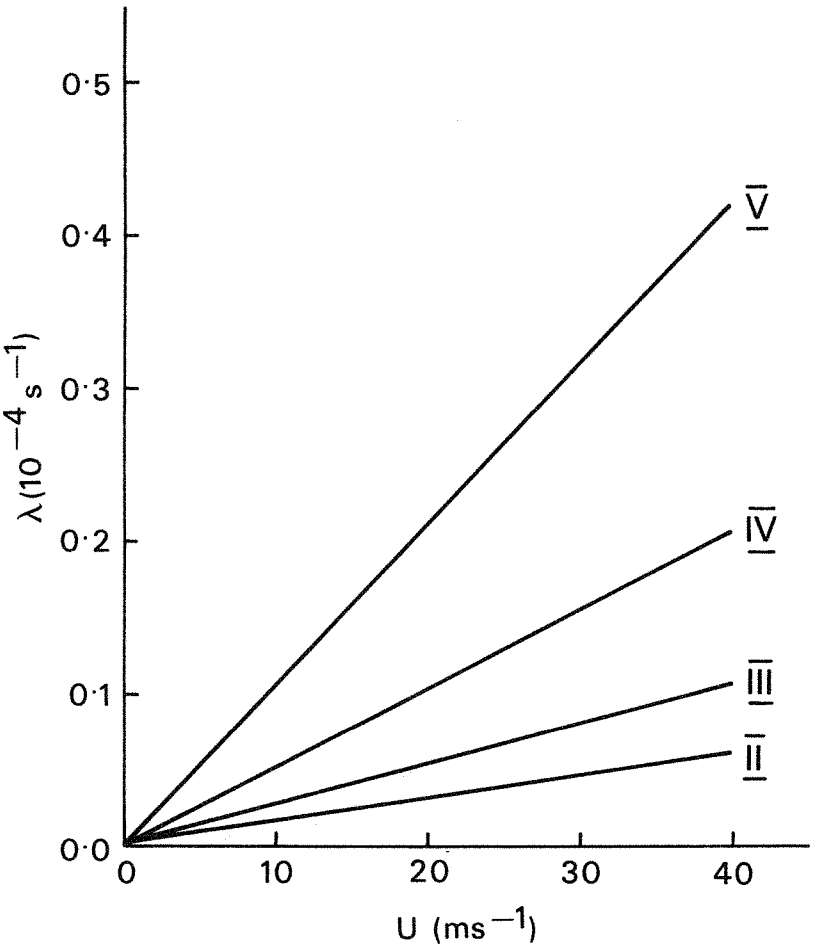

Fig. 9 As Fig. 8 for N = 4.

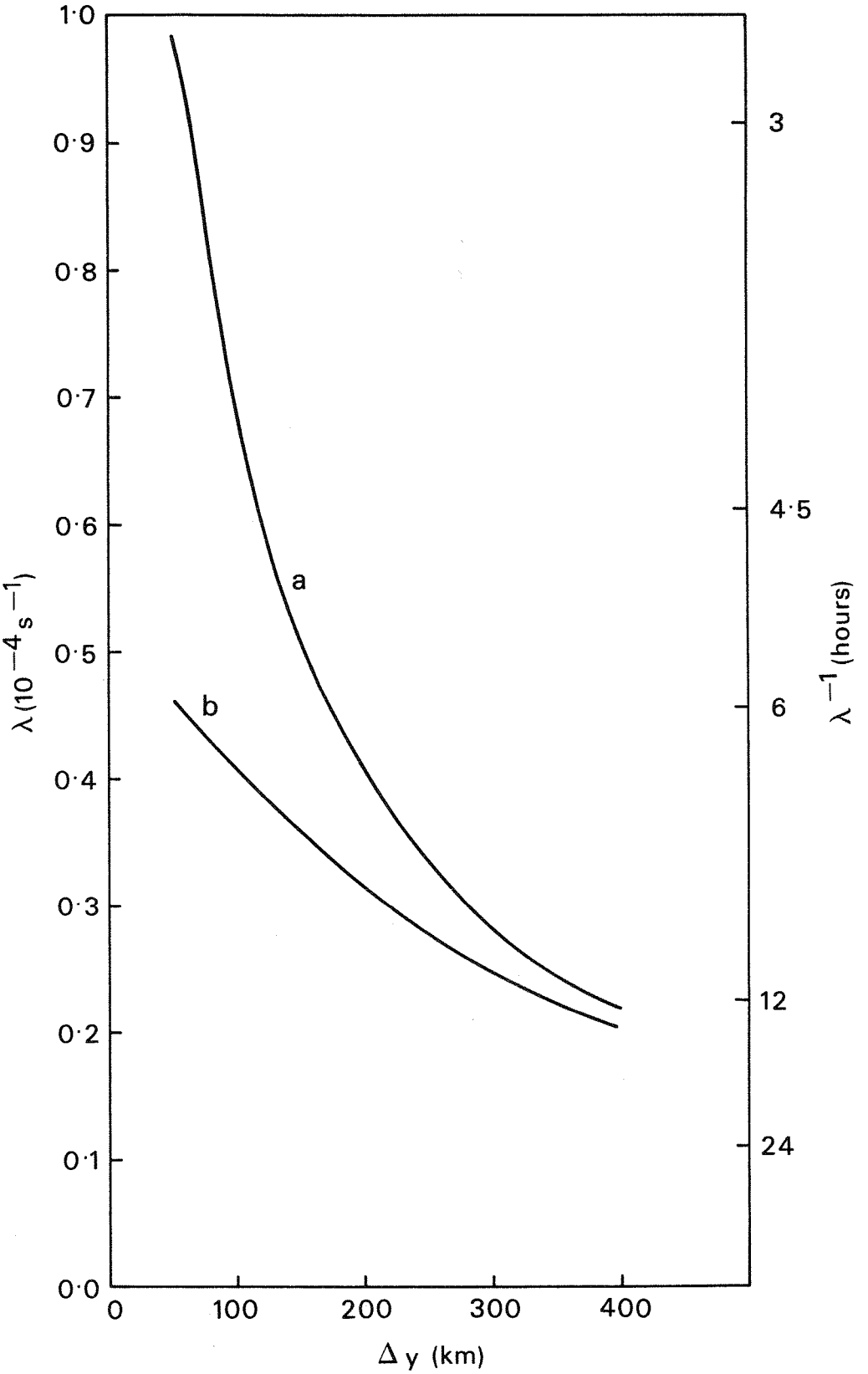

Fig. 10 Variation of growth rate with Δy for $N = 4$ and $\bar{U} = 40\ ms^{-1}$

a) nine level model with GFDL distribution of levels

b) model with 5 equally spaced levels.

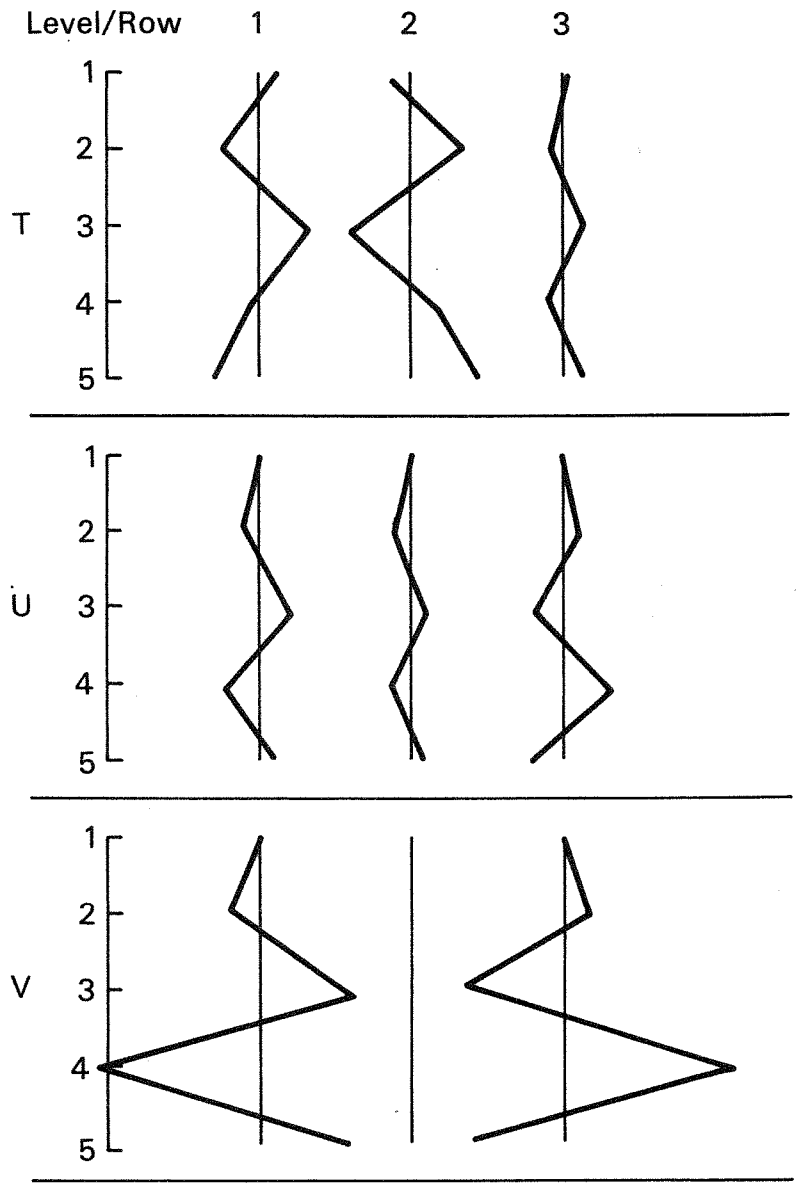

Fig. 11 Structure as a function of height and latitude of T', U', V' for the most unstable mode in a five level model with $\bar{U}$ = 40 ms^{-1}, Δy = 100 km, $f = 1.1 \times 10^{-4}$ and N = 3. The e-folding time is 5.8 hours.

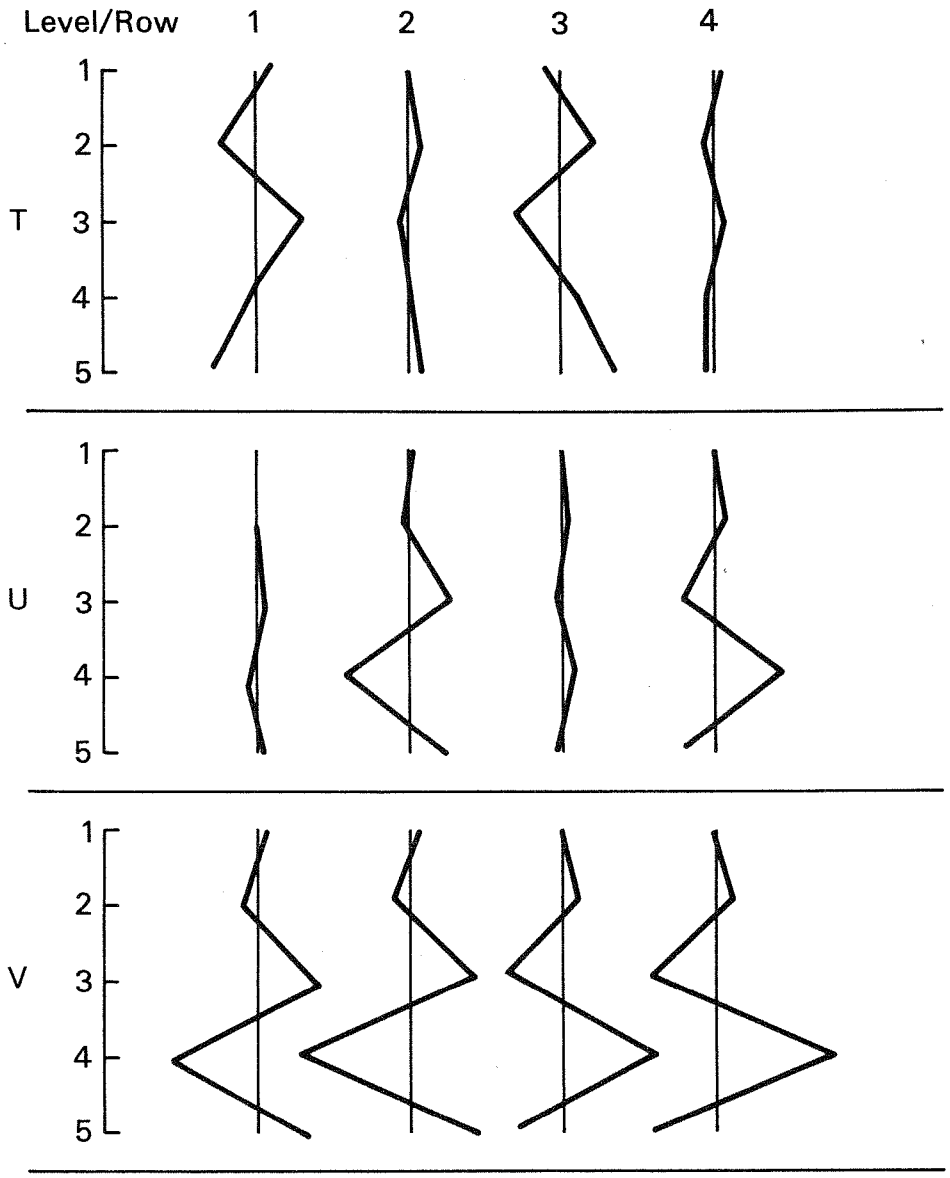

Fig. 12 As Fig. 11 for N = 4. The e-folding time for this mode is 6.6 hours.

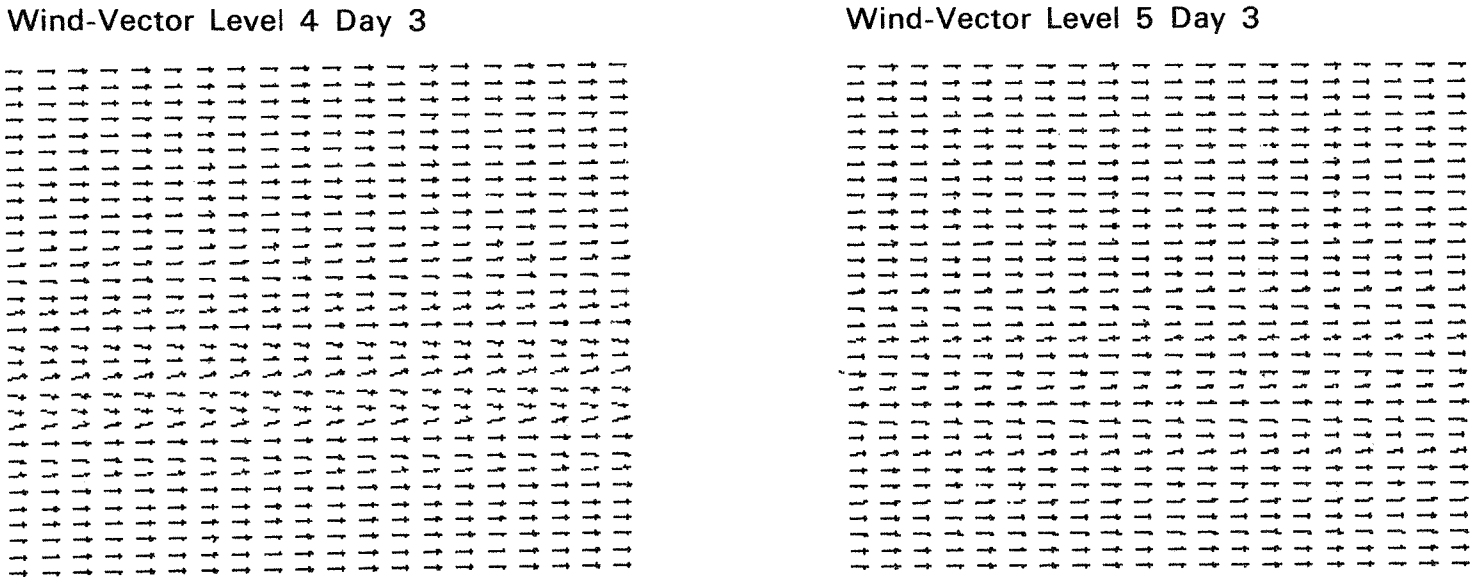

Fig. 13 Wind vectors at levels 4 and 5 at day 3 in a non-linear integration in an f-plane channel. The length of the vectors on the boundary corresponds to 40 ms^{-1}.

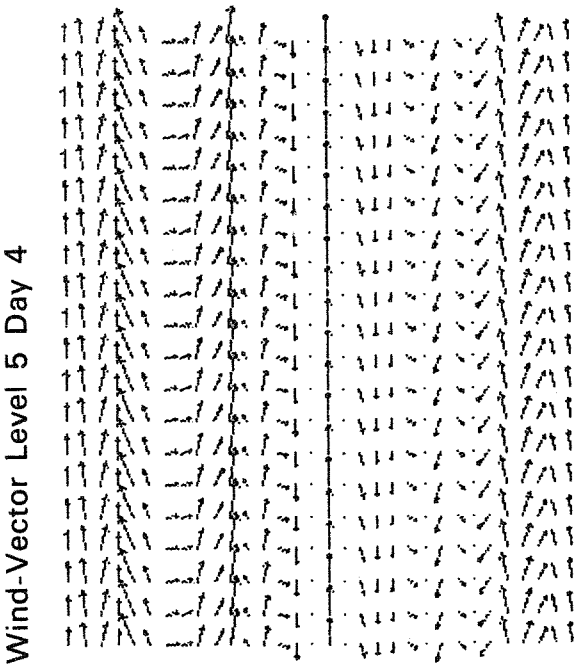

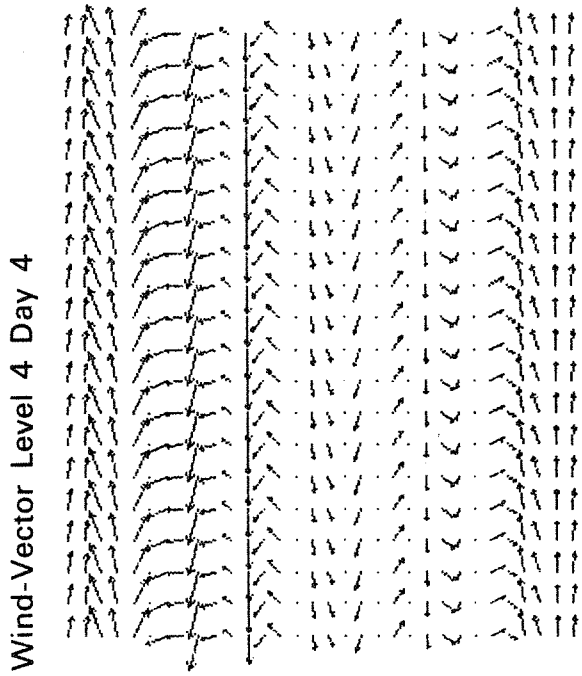

Fig. 14 As Fig. 13 on day 4.

EUROPEAN CENTRE FOR MEDIUM RANGE WEATHER FORECASTS

Research Department (RD)

Internal Report No.22

No. 1 Users Guide for the GFDL Model (November 1976)

No. 2 The effect of Replacing Southern Hemispheric Analyses by Climatology on Medium Range Weather Forecasts (January 1977)

No. 3 Test of a Lateral Boundary Relaxation Scheme in a Barotropic Model (February 1977)

No. 4 Parameterization of the Surface Fluxes (February 1977)

No. 5 An Improved Algorithm for the Direct Solution of Poisson's Equation over Irregular Regions (February 1977)

No. 6 Comparative Extended Range Numerical Integrations with the ECMWF Global Forecasting Model 1 : The N24, Non-Adiabatic Experiment (March 1977)

No. 7 The ECMWF Limited Area Model (March 1977)

No. 8 A Comprehensive Radiation Scheme designed for Fast Computation (May 1977)

No. 9 Documentation for the ECMWF Grid-Point Model (May 1977)

No. 10 Numerical Tests of Parameterization Schemes at an Actual Case of Transformation of Arctic Air (June 1977)

No. 11 Analysis Error Calculations for the FGGE (June 1977)

No. 12 Normal Modes of a Barotropic Version of the ECMWF Grid-Point Models (July 1977)

No. 13 Direct Methods for the Solution of the Discrete Poisson Equation : Some Comparisons (July 1977)

No. 14 On the FACR (ℓ) Algorithm for the Discrete Poisson Equation (September 1977)

No. 15 A Routine for Normal Mode Initialization with Non-Linear Correction for a Multi-Level Spectral Model with Triangular Truncation (August 1977)

No. 16 A Channel Version of the ECMWF Grid-Point Model (December 1977)

No. 17 A Comparative Study of Some Low Resolution Explicit and Semi-Implicit Spectral Integrations (August 1978)

EUROPEAN CENTRE FOR MEDIUM RANGE WEATHER FORECASTS

Research Department (RD)

Internal Report No.22

No. 18 Verification and storing with empirical orthogonal functions (November 1978)

No. 19 Documentation of the ECMWF Spectral Model (October 1978)

No. 20 A study of the effect of an interactive radiation scheme on a medium range forecast (December 1978)

No. 21 Fast Fourier Transforms on Cray-1 (January 1979)

No. 22 Spurious energy conversions in an energy/enstrophy conserving finite difference scheme (February 1979)